Supplementary material

Core-Shell Cu@Cu_2O Nanoparticles Embedded in 3D Honeycomb-like N-Doped Graphitic Carbon for Photocatalytic CO_2 Reduction

Lang He[a], Wenyuan Zhang[b], Kristin Zhao[c], Sheng Liu, [a] Yan Zhao[a]**

[a] *The Institute of Technological Sciences, Wuhan University, Wuhan, 430072, P. R. China.*

[b] *School of Chemistry and Chemical Engineering, Harbin Institute of Technology, Harbin, 150080, P. R. China*

[c] *Lynbrook High School, San Jose, CA 95129*

* Corresponding author

E-mail: victor_liu63@vip.126.com (S. Liu); yan2000@whut.edu.cn (Y. Zhao)

Table of Contents

Time-resolved transient PL measurement

Fluorescence lifetime and steady-state spectrometer (FLs980, Edinburgh Instruments, UK) was used to test the steady-state lifetime photoluminescence (PL) spectrum and time-resolved photoluminescence (TRPL) spectrum, and the excitation wavelength was 384 nm. The emission decay data were fitted to a double-exponential model and the emission decay behavior is deduced through Eq. (1)

$$\boldsymbol{\tau_{avrg.}} = \frac{A_1\tau_1{}^2+A_2\tau_2{}^2}{A_1\tau_1+A_2\tau_2} \quad (1)$$

where τ and A are the decay time and the relative magnitude of components, respectively, and $\tau_{avrg.}$ is the intensity-averaged lifetime used for an overall comparison. The fitting results show the fast decay component (τ_1 and A_1) and the minority-slow component (τ_2 and A_2), decaying from the free excited states and the bound excited states, respectively.

CO_2 Product Selectivity Calculation:

According to the electron transfer number for producing each reduction product ($8e^-$ for CH_4 and $2e^-$ for CO), the selectivity of CH_4 is defined as follows:[1]

$$\mathbf{CO\ (selectivity\ \%)} = \frac{Yield_{(CO)} \times 2}{Yield_{(CO)} \times 2 + Yield_{(CH4)} \times 8} \times 100\%$$

$$\mathbf{CH4\ (selectivity\ \%)} = \frac{Yield_{(CH4)} \times 8}{Yield_{(CO)} \times 2 + Yield_{(CH4)} \times 8} \times 100\%$$

Apparent Quantum Yield values measurement.

Apparent quantum Yield (AQY) values were calculated using the following equation:[2, 3]

$$\mathbf{AQY} = \frac{\text{number of reacted electrons}}{\text{number of incident photons}} \times 100\%$$

The external quantum efficiency values for CO and CH_4 generation were determined at 420 nm using a band pass filter with the same photochemical experimental setup. The flux of incident

photons from the power was measured by a power meter (PL-MW2000, Photoradiometer). The lamp intensity at 420 nm was measured to be 3.97 W·cm^2, the illuminated area was 28.71 cm^2, and the incident photons flux was calculated to be 4777.92 h^{-1}.

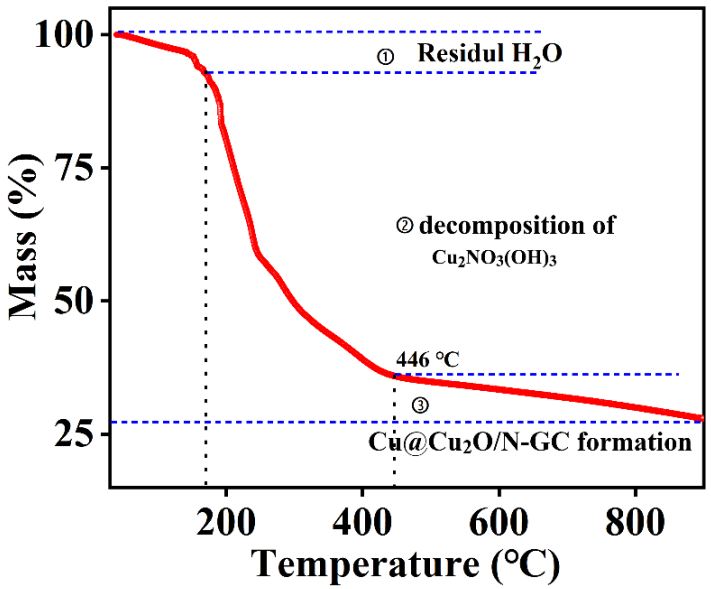

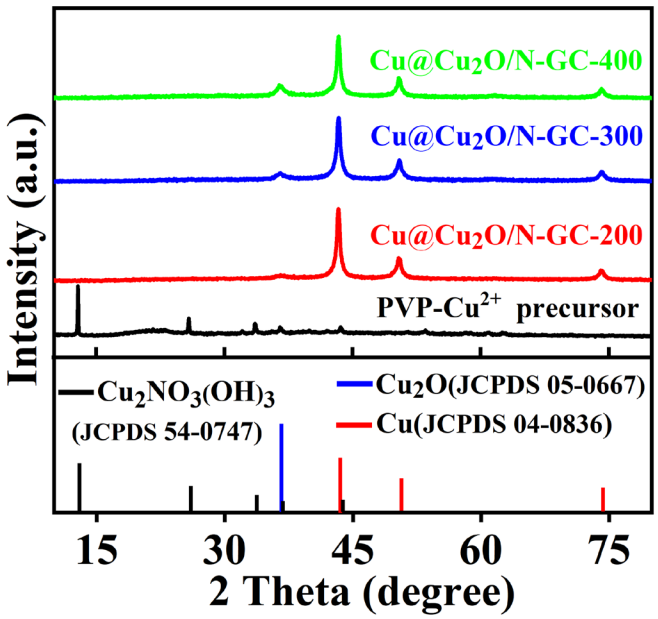

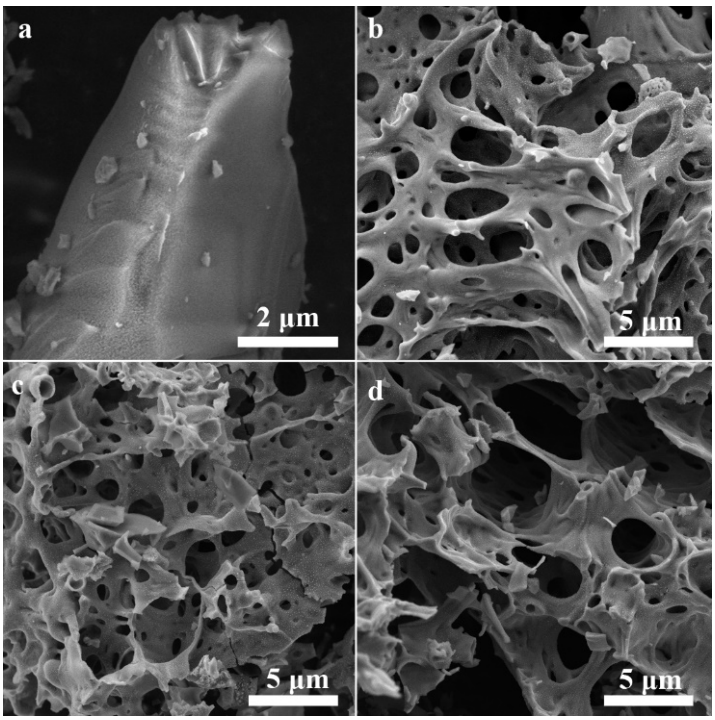
a
2 μm
b
5 μm
c
5 μm
d
5 μm

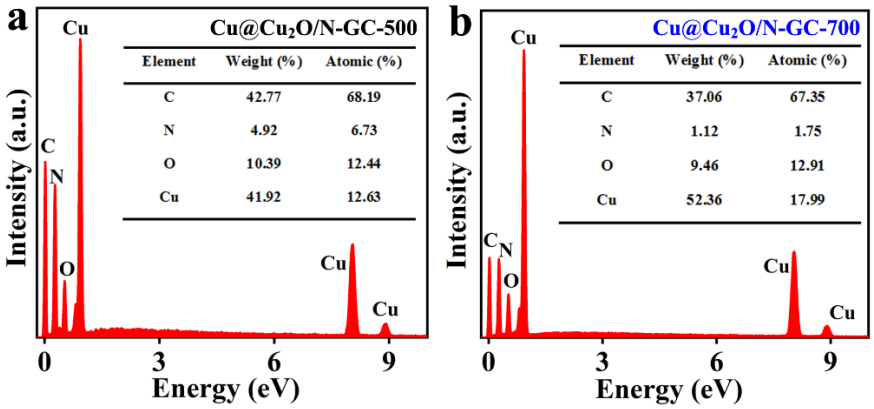
a
Cu@Cu2O/N-GC-500
Element Weight (%) Atomic (%)
C 42.77 68.19
N 4.92 6.73
O 10.39 12.44
Cu 41.92 12.63
Intensity (a.u.)
Energy (eV)
b
Cu@Cu2O/N-GC-700
Element Weight (%) Atomic (%)
C 37.06 67.35
N 1.12 1.75
O 9.46 12.91
Cu 52.36 17.99
Intensity (a.u.)
Energy (eV)

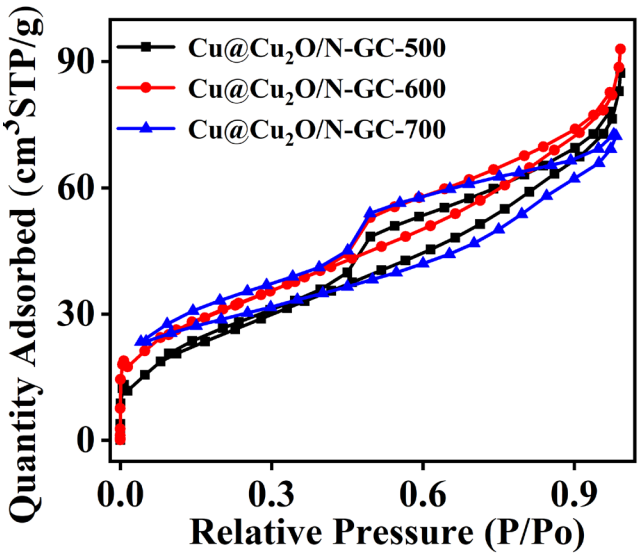
Cu@Cu2O/N-GC-500
Cu@Cu2O/N-GC-600
Cu@Cu2O/N-GC-700
Quantity Adsorbed (cm3STP/g)
90
60
30
0
0.0
0.3
0.6
0.9
Relative Pressure (P/Po)

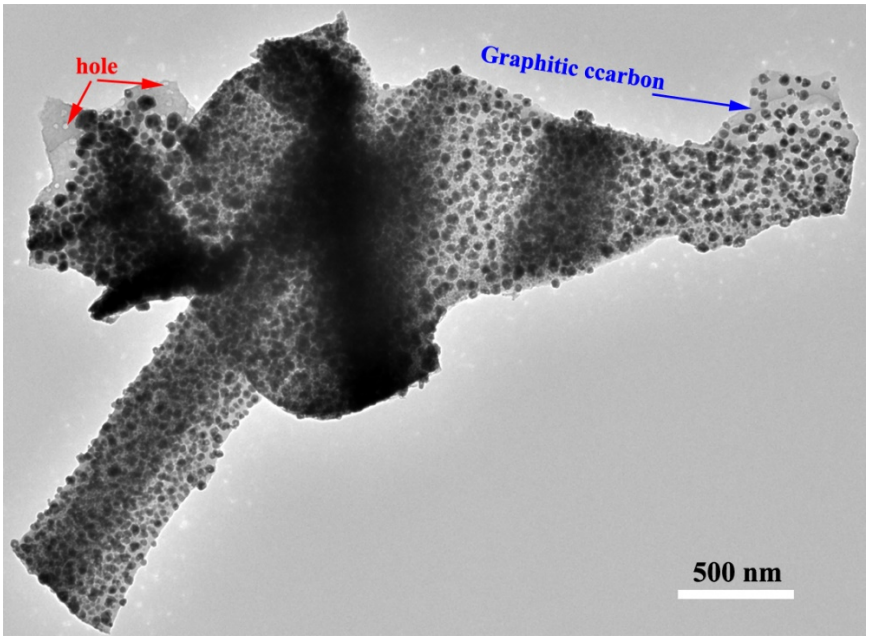
hole
Graphitic ccarbon
500 nm

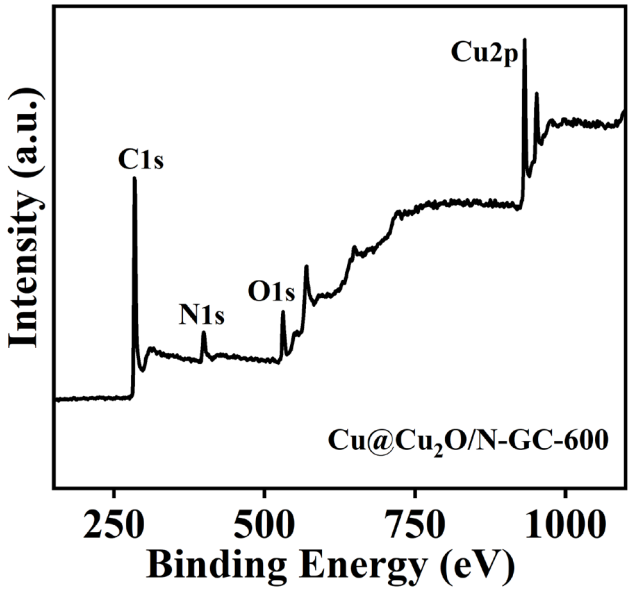

Figure S7 XPS survey spectra of the Cu@Cu_2O/N-GC-600

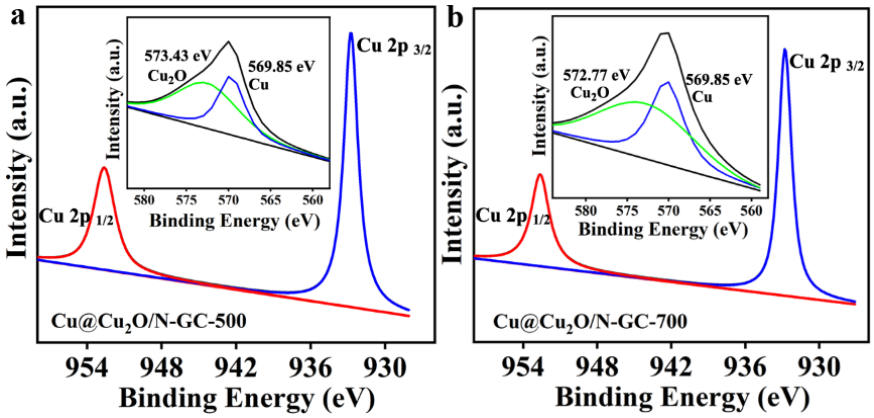

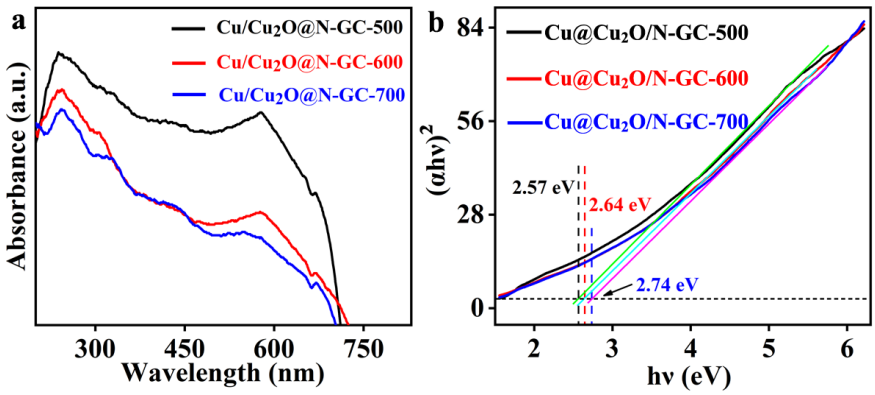
a
Cu/Cu2O@N-GC-500
Cu/Cu2O@N-GC-600
Cu/Cu2O@N-GC-700
Absorbance (a.u.)
300
450
600
750
Wavelength (nm)
b
Cu@Cu2O/N-GC-500
Cu@Cu2O/N-GC-600
Cu@Cu2O/N-GC-700
(αhv)2
84
56
28
0
2.57 eV
2.64 eV
2.74 eV
2
3
4
5
6
hv (eV)

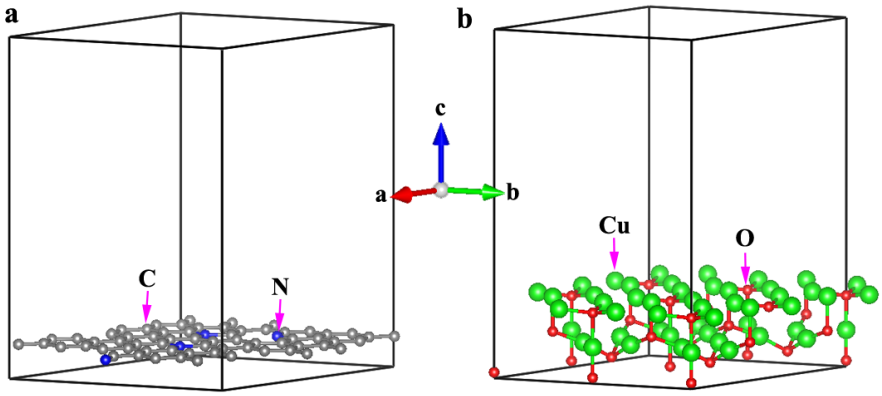
a
C
N
c
a
b
b
Cu
O

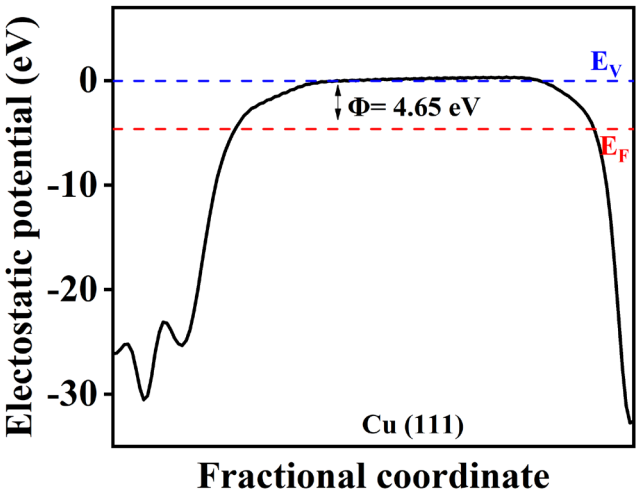
Electostatic potential (eV)
0
-10
-20
-30
E_V
Φ= 4.65 eV
E_F
Cu (111)
Fractional coordinate

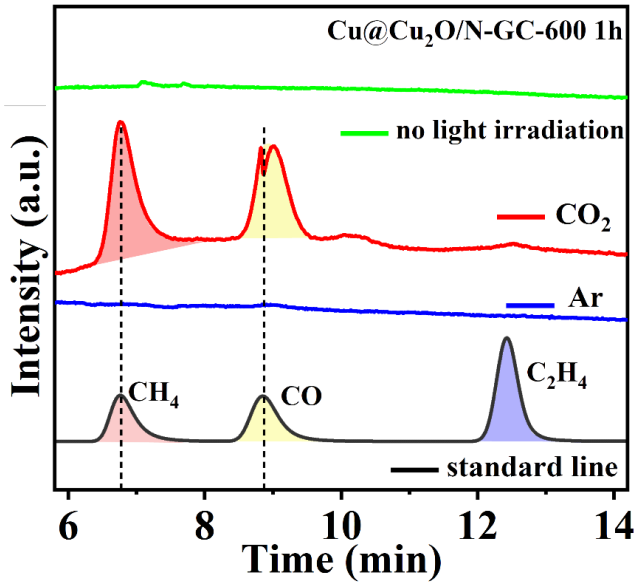
Cu@Cu2O/N-GC-600 1h
no light irradiation
CO2
Ar
C2H4
CH4
CO
standard line
Intensity (a.u.)
6
8
10
12
14
Time (min)

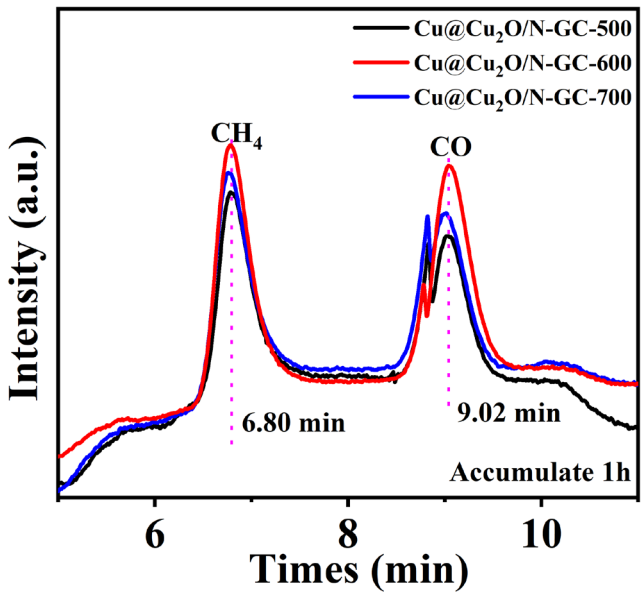
Cu@Cu2O/N-GC-500
Cu@Cu2O/N-GC-600
Cu@Cu2O/N-GC-700
CH4
CO
Intensity (a.u.)
6.80 min
9.02 min
Accumulate 1h
6
8
10
Times (min)

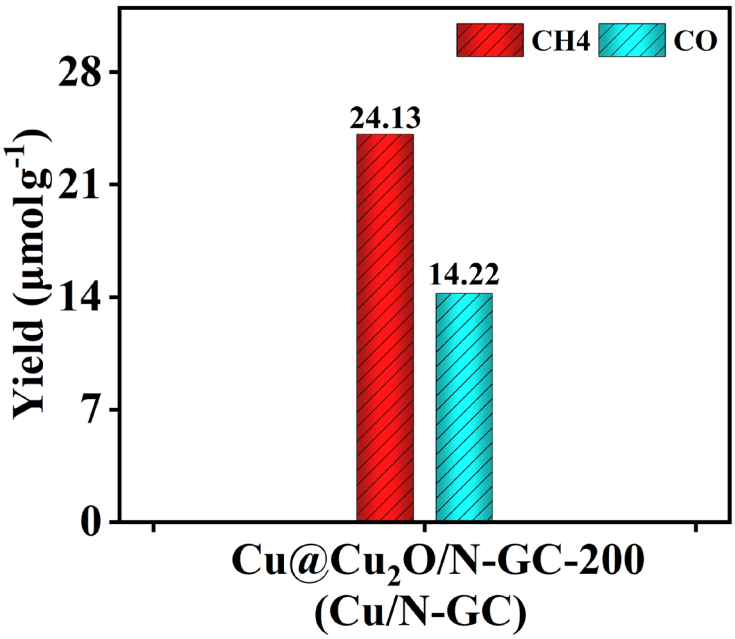
CH4
CO
28
21
14
7
0
24.13
14.22
Yield (μmol g-1)
Cu@Cu2O/N-GC-200
(Cu/N-GC)

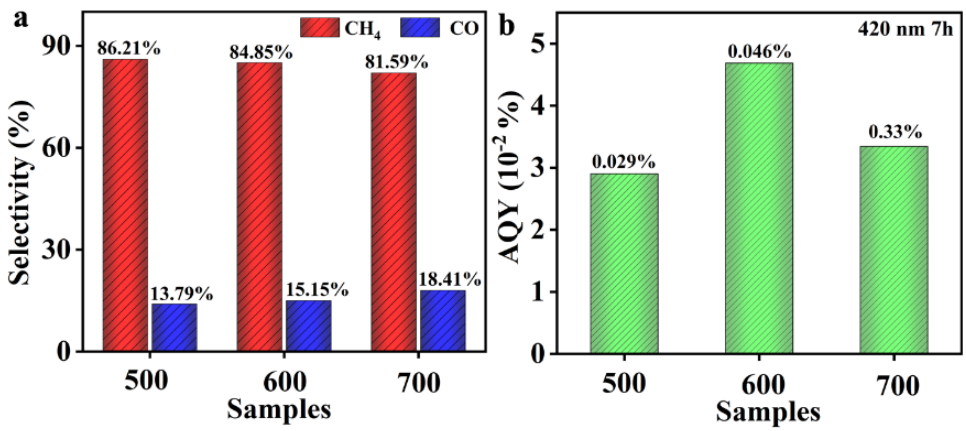

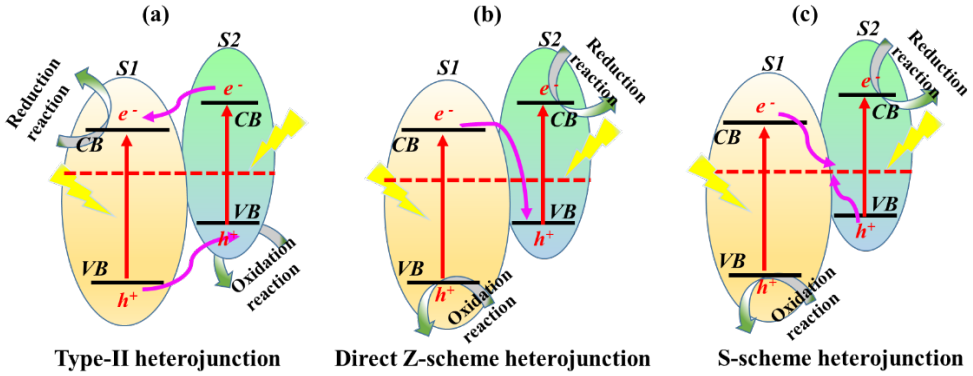

As shown in **Figure S16a**, two semiconductors S1 and S2 with a staggered band structure configuration can form the type II heterojunction, both the CB and VB edges of S2 are higher than those of S1. When the photocatalytic system is excited by light, the photogenerated electrons in the CB of S2 can transfer to the CB of S1 and the photogenerated holes in the VB of S1 can

transfer to the VB of S2 due to the potential difference of CB and VB between the two semiconductors. [4]

In a direct Z-scheme heterojunction **(Figure S16b)**, S1 and S2 are excited by light irradiation, and the photogenerated electrons in the CB of S1 can directly recombine with the holes in the VB of S2. Thus, the photogenerated electrons in the CB of S2 and photogenerated holes in the VB of S1 are spatially separated and also maintain their initial strong redox capability, which enhances the efficiency of the redox reactions. [3].

In an S-scheme heterojunction **(Figure S16c)**, when S1 and S2 come into contact, their Fermi energy should be aligned to the same level. This leads to an upward and downward shift in the Fermi levels of S1 andS2, respectively. The band bending and Coulombic attraction facilitate the recombination of the photogenerated electrons in the CB of S1 and holes in the VB of S2 at the interface region. The active photogenerated electrons and holes are reserved in the CB of S2 and VB of S1, respectively, while the useless photogenerated charge carriers (electrons in CB of S1 and holes in VB of S2) are recombined, resulting a strong redox potential. [5]

As shown in **Figure 9b,** two semiconductors Cu_2O and N-GC with a staggered band structure configuration can form the S-scheme heterojunction, both the CB and VB edges of N-GC are higher than those of Cu_2O and Cu. When the Cu@Cu_2O/N-GC system is excited by light, the photogenerated electrons in the CB of Cu_2O can transfer to the VB of N-GC. As a result, the photogenerated electrons and holes are spatially separated in Cu_2O and N-GC, respectively. The photogenerated electrons in N-GC is used to reduce CO_2. Since the positions of CB of Cu_2O are close to the VB of N-GC, the excited electrons on CB of Cu_2O can further capture the photogenerated holes in the VB of N-GC. The photogenerated electrons and holes in Cu_2O and

N-GC can be spatially separated, which is possibly attributed to the formation of a S-scheme semiconductor heterojunction.[5]

Table S1 Temperature changes during the photocatalytic CO_2 RR under visible light irradiation

Test times (h)	**0**	**1**	**2**	**3**	**4**	**5**	**6**	**7**
Temperature (℃)	24.0	24.3	24.6	24.9	25.0	25.1	25.3	25.3

Table S2 BET results of the Cu@Cu_2O/N-GC catalysts.

Samples	**S_{BET} (m^2/g)**	**pore sizes (nm)**	**pore volumes(cm^3/g)**
Cu@Cu_2O/N-GC-500	37.72	3.43	0.025
Cu@Cu_2O/N-GC-600	89.86	3.80	0.079
Cu@Cu_2O/N-GC-700	49.01	3.43	0.028

Table S3 Fitting parameters for TRPL curves recorded for Cu@Cu_2O/N-GC-500, Cu@Cu_2O/N-GC-600 and Cu@Cu_2O/N-GC-700 samples.

Sample	**τ_1 (ns)**	**% percentage**	**τ_2 (ns)**	**% percentage**	**$\tau_{avrg.}$ (ns)**
Cu@Cu_2O/N-GC-500	0.37	0.64	0.36	0.36	0.36
Cu@Cu_2O/N-GC-600	0.42	0.62	0.42	0.38	0.41
Cu@Cu_2O/N-GC-700	0.44	0.62	0.44	0.38	0.44

Table S4 Cu 2p peak position and peak area ratio (Cu_2O/Cu) of samples

Sample	**$Cu@Cu_2O$/N-GC-500**		**$Cu@Cu_2O$/N-GC-600**		**$Cu@Cu_2O$/N-GC-700**	
Peak	Cu_2O	Cu	Cu_2O	Cu	Cu_2O	Cu
Peak position (eV)	573.43	569.85	573.60	569.20	572.77	570.21
Peak area ratio Cu_2O/Cu	**1.18**		**1.25**		**1.51**	

Table S5. Comparison of the gas photocatalytic performance for the Cu_2O-based photocatalysts reported in the literature.

metal oxide Photocatalysts	**Product and Yield**	**Stability (h)**	**Ref.**
Cu_2O/Ti_3C_2 MXene	CO (17.55 μmol g^{-1} h^{-1}) CH_4 (0.96 μmol g^{-1} h–1)	**17**	6
$Cu_2O@Cu$	CH_4 (0.137 μmol cm^{-2})	**24**	7
Cu_2O/CeO_2	CO (~1,2 μmol g^{-1} h^{-1})	**30**	8
g-C_3N_4 foam/Cu_2O QDs	CO 8.12μmol g^{-1} h^{-1} CH_4 (~0.1 μmol cm^{-2})	**25**	9
Cu_2O decorated WO_3	CH_4 (~10 μmol h^{-1} g^{-1})	**24**	10
$Cu@Cu_2O$/N-GC This work	CO (27.78 μmol g^{-1}) CH_4 (38.89 μmol g^{-1})	**42**	—

References

1. J. Fu, K. Jiang, X. Qiu, J. Yu and M. Liu, *Materials Today*, 2020, **32**, 222-243.
2. Chang, Huang, Xingjiu, Meng, Meng, Qiangqiang, Qunxiang, Wang, Dawei and Zhao, *Advanced Materials*, 2016, **28**, 6485-6490.

3. Y. Lin, Q. Zhang, Y. Li, Y. Liu, K. Xu, J. Huang, X. Zhou and F. Peng, *ACS Sustainable Chemistry & Engineering*, 2020, **8**, 4537-4546.

4. T. Kothe, N. Plumeré, A. Badura, M. M. Nowaczyk, D. A. Guschin, M. R?Gner and W. Schuhmann, *Angewandte Chemie*, 2013, **52**, 14233-14236.

5. Q. Xu, L. Zhang, B. Cheng, J. Fan and J. Yu, *Chem*, 2020, **6**, 1543-1559.

6. J. Zhang, J. Shi, S. Tao, L. Wu and J. Lu, *Appl. Surf. Sci.*, 2020, **542**, 148685.

7. J. Zhou, Y. Li, L. Yu, Z. Li, D. Xie, Y. Zhao and Y. Yu, *Chem. Eng. J.*, 2020, **385**, 123940.

8. Y. Pu, Y. Luo, X. Wei, J. Sun, L. Li, W. Zou and L. Dong, *Appl. Catal. B Environ.*, 2019, **254**, 580-586.

9. Z. Sun, W. Fang, L. Zhao, H. Chen, X. He, W. Li, P. Tian and Z. Huang, *Environment International*, 2019, **130**, 104898.

10. W. Shi, X. Guo, C. Cui, K. Jiang, Z. Li, L. Qu and J.-C. Wang, *Appl. Catal. B Environ.*, 2019, **243**, 236-242.